



## MODIFICATION OF GLOBAL PROPERTIES OF A MIXING LAYER BY OPEN/CLOSED LOOP ACTUATION

Vladimir Parezanović, Jean-Charles Laurentie, Carine Fourment, Laurent Cordier, and Bernd R. Noack

Departement Fluides, Thermique, Combustion  
Institut PPRIME, CNRS UPR 3346  
CEAT, 43 rue de l'Aerodrome, F-86036 Poitiers, FRANCE  
vladimir.parezanovic@univ-poitiers.fr

**Tamir Shaqarin**  
Mechanical Engineering Department, College of Engineering  
Tafila Technical University  
JORDAN

### ABSTRACT

Open- and closed-loop control of a turbulent mixing layer is experimentally performed in a dedicated large scale, low speed wind-tunnel facility. The flow is manipulated by fluidic micro-jet actuators integrated in the trailing edge of the splitter plate. Sensing is performed using a rake of hot-wire probes downstream of the splitter plate in the mixing layer. The control goal is the manipulation of the spreading rate and of the virtual origin of the mixing layer. The underlying physical mechanisms employ a wide range of frequencies. The calculated Reynolds number based on momentum thickness of the boundary layer at the trailing edge is around  $Re=500-2000$  depending on the mixing layer configuration. Control authority is presented using smoke visualization, Particle Image Velocimetry (PIV) and hot-wire measurements of local velocity.

### Introduction

Controlling the mixing layer properties such as initial transition, turbulence level, expansion rate, redistribution and mixing is a problem largely addressed in the literature in the past several decades. Passive parameters such as the shape of the trailing edge, the presence of initial spanwise perturbation, the external turbulence level or the presence of longitudinal pressure gradients can have a large influence on the mixing layer downstream evolution (Fiedler, 1998; Mathis, 2006; Perret, 2004). In a zero pressure gradient configuration numerous experiments have been performed leading to a doubling of the expansion rate of the mixing layer. Open loop active flow control using acoustical perturbations in the plenum chamber, vibrating trailing edge, or synthetic jets at the wall have been performed. It can be based on the excitation of the most amplified initial perturbations that can be directly related to the initial momentum thickness of the boundary layer over the splitting plate (Ho & Huerre, 1984), based on relatively low frequency large scales (Fiedler, 1998), or at very high frequencies (Wiltse & Glezer, 1993).

By nature the mixing layer is very receptive to every

perturbation and behaves as an amplifier of these perturbations. On the other hand the mixing layer is driven by convective instabilities. These considerations make a closed-loop control and optimization of this control of the mixing layer challenging. Some open questions remain that closed-loop control could answer: Can we do more than doubling the expansion? How far downstream does an eventual modification of the expansion last? While the mixing layer is continuously growing in its downstream evolution, a wide range of large scales are present, therefore actuating at a given frequency should promote some local reorganization of the flow?

Developments of modern actuators as micro-valves, piezoelectric, synthetic jets, plasmas, etc. and of real-time systems with a large input/output data rate and computational power makes it possible to envisage such close-loop control to be performed.

In this paper we present a preliminary study based on a specially designed mixing layer wind-tunnel whose main features are low speeds and large scale in such a way that the dimensions, typical frequency response and authority of the available actuators and the typical performances of real-time system can address the configuration. By using an open-loop strategy, and a parametric approach, we first show that the mixing layer is receptive to the periodic perturbations injected through micro-jets located at the trailing edge of the splitter plate. The perturbations at low frequency creates a doubling of the expansion of the flow. The analysis of the experimental results shows that we can hope to monitor the downstream distance up to which this doubling occurs. Finally, by using a simple feedback approach where the local organization of the flow, obtained by a POD approach (Lumley, 1967), at a given streamwise location is used to trigger the perturbations. A synchronization occurs that enhance this local organization.

## Experimental setup

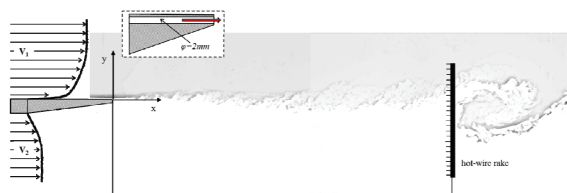


Figure 1. Mixing layer experiment configuration.

The mixing layer is composed of two independent streams generated by the wind tunnel, specifically built for the purpose of this experiment. The test section has a square cross-section of  $1\text{m} \times 1\text{m}$  and is 3m long. A porous diffuser is used at the outlet of the test section in order to prevent external perturbations. Each stream can be driven independently in a range of velocities  $[0.5 : 12]\text{m/s}$ . The two streams meet at the end of a splitter plate which is 80mm thick at the start, and 3mm at the trailing edge. The taper is introduced only on the lower velocity side of the splitter plate which is angled at  $8^\circ$ , while the upper surface is horizontal, as can be seen in Fig. 1. A head loss device (foam) is placed on the low velocity side upstream of the bevel in order to stabilize the low velocity stream. The trailing edge contains 96 circular cross section nozzles of diameter 2mm along its span. Each of them is individually connected to a micro valve actuator. Each of the micro valves can be controlled separately. However in the present study, only a spanwise mode 0 is actuated and they all are driven by a common signal which is a square wave signal of adjustable frequency and duty cycle. The 96 actuators are capable of frequencies higher than 800Hz and of mean exit velocities of the order of the convection velocity of the mixing layer flow, blowing in the streamwise direction. The velocity response of the jets was characterized with a single miniature hot-wire probe positioned 1mm downstream of the trailing edge. At low actuation frequencies the velocity response contains strong transients, while at higher frequencies a response close to a sinusoidal wave is obtained. This is not an issue for the present study, but will be in later stages of the project when these non-linear effects will have to be considered when designing the transfer function for a closed loop control. The actuators are fed from a common reservoir which is also situated in the splitter plate. The pressure inside this reservoir is controlled automatically which maintains a constant amplitude of the jet nozzle exit velocity, for any actuation frequency and duty cycle setting. Measurements comprise Particle Image Velocimetry (PIV) using two Lavisson Image Pro PIV cameras with an acquisition rate of 5Hz, and local velocity measurements using a rake of 24 hot-wire probes which can be displaced in a  $xOy$  plane from  $X=50$  to 1500mm in streamwise, and  $Y = \pm 230\text{mm}$  in transversal directions. The outer hot-wires in the rake are 184 mm apart; hence, the rake can cover from 0.5 to 4 times the local vorticity thickness of the baseline flow, depending on its streamwise location. Data acquisition and control are performed by using a *Concurrent iHawk* real-time system.

Our current experiment is set up for two different conditions of the mixing layer flow. These configurations will be denoted as "LS" (low speed) and "HS" (high speed) mixing layers. In the LS configuration, the velocity parameters are  $U_a=4.7\text{m/s}$  and  $U_b=1.2\text{m/s}$  leading to a ve-

locity ratio  $r=0.255$  and a convective velocity  $U_c=3.45\text{m/s}$ , while in the HS configuration they are  $U_a=9\text{m/s}$ ,  $U_b=1.5\text{m/s}$ ,  $r=0.166$  and  $U_c=5.25$ . The boundary layer on the upstream plate of the high speed side of the mixing layer is turbulent (LS:  $\delta_{99}=6.9\text{mm}$ ,  $\theta=0.73\text{mm}$  and  $H=2.44$ ; HS:  $\delta_{99}=13.3\text{mm}$ ,  $\theta=0.82\text{mm}$  and  $H=1.51$ ). The boundary layer on the low velocity side is always less than 1mm in thickness.

The results presented here aim at confirming the control authority over the basic features of the mixing layer and establishing a relevant criterion for a state-detection feedback signal. The micro jets are actuating on the spanwise mode 0; all of them are activated in unison, therefore limiting the forcing to mainly 2D dynamics of the mixing layer. The actuation duty cycle is set at 50% and the effects are explored for a range of actuation frequencies, from 5Hz to 400Hz.

Based on the initial sum of the momentum thicknesses of boundary layers, and the convective velocity, an initial Reynolds number of around  $Re \sim 500$  can be estimated for the LS mixing layer. The natural mixing layer stays laminar a good distance downstream of the origin before beginning its transition to turbulence. An estimated Reynolds number for the HS configuration is  $Re \sim 2000$ , and in this case a turbulent upper boundary layer generates a fully turbulent mixing layer immediately downstream of the trailing edge.

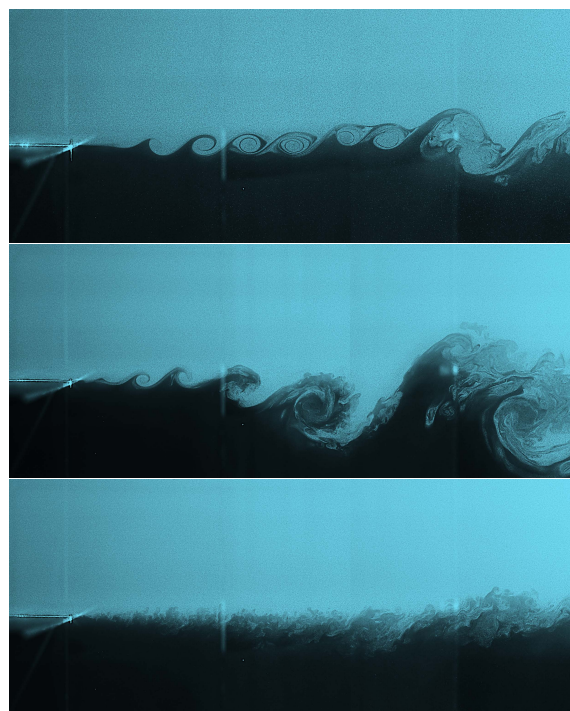


Figure 2. Visualisation of the low speed configuration. From top to bottom : base line, actuation at  $f_a=10\text{Hz}$  and actuation at  $f_a=400\text{Hz}$ . The field of view covers  $X=0$  to 440mm.

## PIV measurements

The PIV cameras are positioned so that the initial part of the developing mixing layer can be observed: from the trailing edge to around 440mm downstream. A transition

August 28 - 30, 2013 Poitiers, France

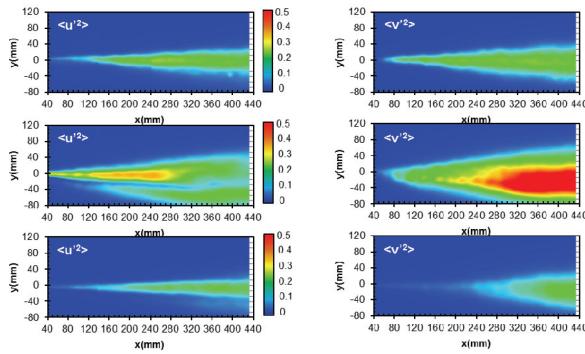


Figure 3. Example of Influence of the actuation frequency  $f_a$  on the turbulence in the area close to the trailing edge of the splitting plate. Low speed case. From top to bottom: base line,  $f_a=10$  and  $f_a=400$  Hz.

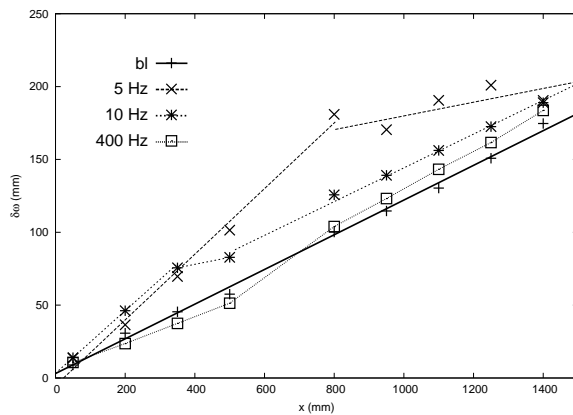


Figure 4. Influence of the actuation frequency  $f_a$  on the vorticity thicknesses  $\delta_{\omega}$ .

from laminar to turbulent flow is observed in this region, the exact point of transition depending on the actuation frequency. Visualization in Fig. 2 shows the three selected configurations of the mixing layer: a) baseline flow, b) actuation at 10Hz and c) actuation at 400Hz. Visualization of the baseline flow reveals six periods of Kelvin-Helmholtz vortices after which the vortex pairing occurs, leading to a change in the expansion rate of the mixing layer. The natural frequency of the mixing layer in the region of the laminar vortices is  $f_{lam} \sim 90$ Hz. Consequently, in the case of  $f_a=10$ Hz, vortex pairing is forced by the actuating jet and the mixing layer starts to increase its spreading rate much more rapidly. The visualization for the case of actuation at  $f_a=400$ Hz shows a fully turbulent mixing layer. No large structures are visible any longer and the interface between the two streams consists of small scale turbulence.

These observations are corroborated by mean velocity and mean velocity fluctuation fields shown in Fig. 3. A strong increase of vertical fluctuations is observable for the case of  $f_a=10$ Hz. The case of  $f_a=400$ Hz case looks very similar to the baseline flow in terms of the spreading rate and the level of mean fluctuations. However, thanks to visualization we know that these two flows are very different in their nature.

## Hot-wire rake measurements

Hot wire rake has been used to recover local mean velocity and mean velocity fluctuation profiles in  $xOy$  planes at various locations downstream of the trailing edge. From these velocity profiles we can observe the evolution of vorticity thickness, shown in Fig. 4 for the LS mixing layer configuration. The baseline flow shows a linear evolution of vorticity thickness, with a slope of  $\frac{\partial \delta_{\omega}}{\partial x} = 0.119$ . The low frequency actuation of  $f_a=5$ Hz and  $f_a=10$ Hz both double the initial vorticity thickness growth rate until  $X=800$ mm in the former and  $X=350$ mm in the latter case. The high frequency actuation  $f_a=400$ Hz initially reduces the vorticity growth rate, but further downstream at around  $X=800$ mm, the growth rate changes again, the vorticity thickness becomes higher compared to the baseline flow, but the growth rates are similar in both cases.

These results correspond well with the fact that the actuation affects the transition point of the laminar part of the mixing layer. For the low frequency actuation, the initial part of the mixing layer is dominated by large structures which are created by the tendency of the flow to synchronize itself to the actuation frequencies. This synchronization can be observed in Fig. 6, from the spectral maps of the baseline flow and various actuation frequencies  $f_a$  for both LS and HS mixing layer configurations. For the streamwise measurement positions shown in Fig. 6(LS), the baseline flow of LS configuration features energy contained in the low frequency range (2-10Hz). For low frequencies of actuation  $f_a=5$ Hz and  $f_a=10$ Hz the energy in the spectra becomes concentrated at  $f_a$  until a certain downstream position, where a re-emergence of base flow frequencies appears. For  $f_a=5$ Hz this occurs around  $X=800$ mm which corresponds to the change in vorticity thickness growth rate as shown above. Corresponding change is visible for  $f_a=10$ Hz earlier upstream, at around  $X=350$ mm.

These transition regions in which the vorticity growth rates are changing can also be identified from the distribution of fluctuation energy shown as  $\overline{u'^2}/\Delta U^2$  in Fig. 5. An initial linear growth features energy contained in a single, well defined peak (Fig. 5(a) LS ML, for  $X=200$  to  $500$ mm). In the regions of the first growth rate change, the fluctuation energy profiles feature two or more peaks, as can be seen for  $f_a=5$ Hz between  $X=1000$ mm and  $X=1400$ mm. Around  $X=1400$ mm for this case, a resurgence of a single-peak profile can be observed, which indicates that far enough downstream this configuration will establish a growth rate similar to baseline, just as is the case with  $f_a=10$ Hz in Fig. 5(c) between  $X=500$ mm and  $X=800$ mm.

The higher actuation frequencies reduce the initial fluctuation energy as can be seen in Fig. 5(d) and (e), compared to the baseline flow for the LS configuration. This corresponds to the reduced initial vorticity thickness growth rate, as seen in Fig. 4. High actuation frequency is not able to synchronize the mixing layer as low actuation frequencies do; instead the momentum injected in this way into the mixing layer diffuses as a part of the turbulence cascade.

The HS configuration of the mixing layer largely behaves in the same way as described for the LS configuration. Fig. 6(HS) shows synchronization for  $f_a=5$ Hz and 10Hz, but this occurs much farther downstream for 5Hz than in the LS configuration. The case of  $f_a=10$ Hz shows appearance of base flow frequencies around  $X=500$ mm after which the fluctuation energy profile in Fig. 5(c) HS ML) indicates a vorticity growth rate change, which is confirmed from vorticity thickness measurements in that region (not shown in

this article).

### Close loop selection of optimal actuation frequency

The Proper Orthogonal Decomposition (POD) of the hot wire signals in real time, can provide some efficient feedback information for selecting the optimal frequency to be applied for synchronizing the mixing layer. For a given streamwise location of the hot-wire rake in the mixing layer, a POD is first performed on a time history  $u(y_i, t)$  of the base line un-actuated flow. These signals are decomposed as:  $u(y_i, t) = \sum_j^N a_n(t) \Phi^{(n)}(y_i)$ , where  $N$  the number of POD modes is the number of hot-wires used in the rake. Real time signals can then be projected onto the first POD  $\Phi^{(1)}$  in such a way that real time estimates of projection coefficient  $a_j(t)$  is obtained  $a_j(t) \propto \sum_{i=1}^N u(y_i, t) \Phi^{(1)}(y_i)$ . One individual POD coefficient (e.g. coefficient  $a_1(t)$ ) can then be isolated. A threshold  $a_{th}$  is introduced to generate a square signal  $S_q(t) = 1$  if  $a_1(t) > a_{th}$ , and is fixed in such a way that  $prob(S_q > 1) = prob(S_q \leq 1)$  and drives directly the upstream actuation. This strategy has been applied successfully to the mixing layer as illustrated Fig. 7. From the visualizations of the base line configuration (first row of this figure) some organization of the flow can be evidenced. Clearly (from row 2), the feedback procedure automatically extracts from the POD coefficient a *self-triggering mode* that synchronizes the flow at the characteristic frequency naturally present at the streamwise rake-location. A spectral analysis of the feedback signal leads to a dominant frequency. This frequency is in a third stage applied to perform an open-loop control (row 3).

### Conclusions

The experimental investigation performed shows that the system of actuators has a good control authority over the basic features of both transitional and fully turbulent mixing layer configurations.

The actuation provokes different effects on the mixing layer properties with regard to its streamwise evolution. The initial "perturbed" part of the mixing layer will experience either an increased (up to double) or a decreased vorticity thickness growth rate, depending on the actuation frequency. For a given frequency of actuation, the flow will be synchronized at  $f_a$  until a downstream position at which the natural local frequency  $f_n(X)$  of the un-actuated mixing layer is equal to the frequency of actuation  $f_a$ . At this point the mixing layer begins a transition into a state similar to the un-actuated flow corresponding to this point, which

results in the actuated mixing layer obtaining a growth rate similar to that of the baseline flow (but not necessarily the same local vorticity thickness). Both mixing layer configurations behave in generally the same manner, the differences being the streamwise locations of the growth rate transition regions. These differences come as a result of the different nature of the flow in the two configurations (initially laminar in LS and fully turbulent in HS), where the LS configuration features an additional degree of freedom in the form of a laminar-turbulent transition point which shifts depending on the frequency of actuation.

Finally, by using a simple feedback approach where the local organization of the flow, obtained by a POD approach, at a given streamwise location is used to trigger the perturbations. A synchronization occurs that enhance this local organization, and comes as a direct consequence of the natural spatial selection of the dominant frequency of the flow inherent in the unperturbed mixing layer. This effectively means that with this type of feedback control no previous parametric study is necessary for revealing the optimal parameters; the flow itself will feed back the optimal actuation frequency. This self-synchronization implies a linear mechanism in otherwise highly non-linear problem.

The future work will focus on experimental studies of several closed-loop control approaches such as reference-tracking, machine learning for in-time control, ARX type models, etc.

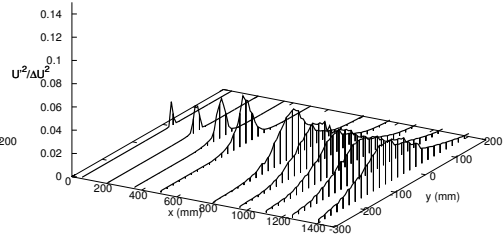
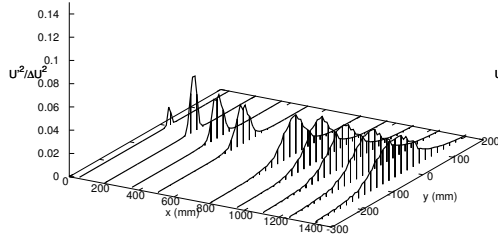
This project is funded by the ANR Chair of Excellence TUCOROM.

### REFERENCES

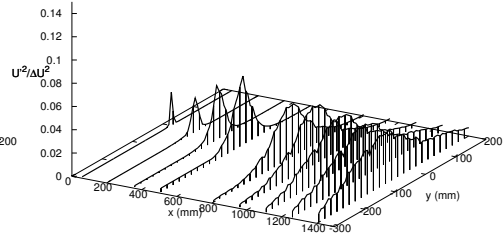
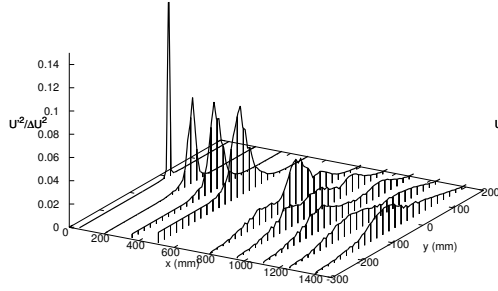
- Fiedler, H. E. 1998 Control of free turbulent shear flow. In *Flow control Fundamentals and Practices* (ed. M. Gad-el Hak, A. Pollard & J. P. Bonnet), pp. 335–429. Springer.
- Ho, C.M. & Huerre, P. 1984 Perturbed free shear layers. *Ann. Rev. of Fluid Mech.* **16**, 365–424.
- Lumley, J. L. 1967 The structure of inhomogeneous turbulent flows. In *Atmospheric Turbulence and Radio Propagation* (ed. V. I. Yaglom & A. M. Tatarsky), pp. 166–178. Moscow: Nauka.
- Mathis, R. 2006 Etude expérimentale du contrôle d'une couche de mélange par décollement pilote. PhD thesis, Université de Poitiers, LEA.
- Perret, L. 2004 Etude du couplage instationnaire calculs-experiences en écoulements turbulents. PhD thesis, Université de Poitiers, LEA.
- Wiltse, J. M. & Glezer, A. 1993 Manipulation of free shear flows using piezoelectric actuators. *J. Fluid Mech.* **249**, 261–285.

a) Base flow LS ML

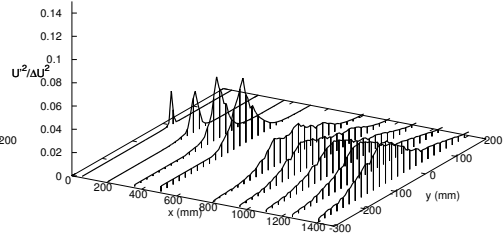
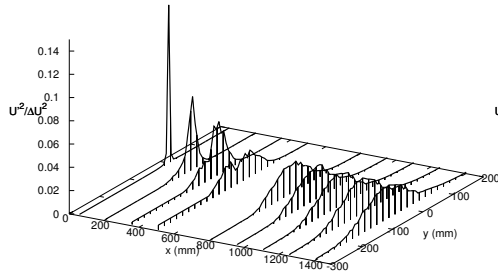
HS ML



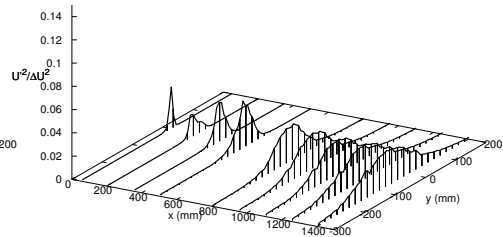
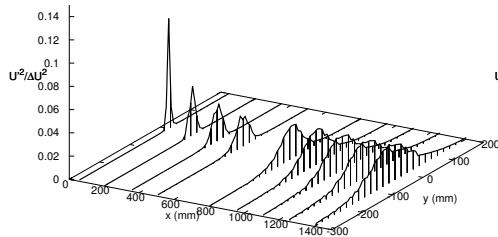
b)  $f_a=5\text{Hz}$



c)  $f_a=10\text{Hz}$



d)  $f_a=60\text{Hz}$



e)  $f_a=400\text{Hz}$

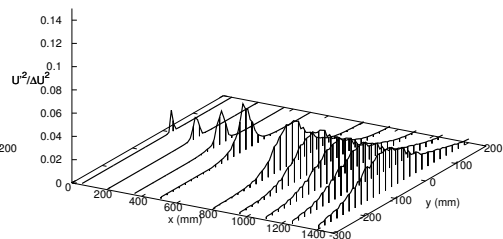
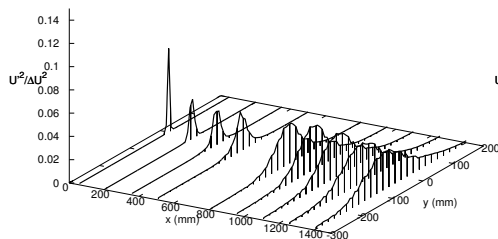


Figure 5. Evolution of the turbulent quantity  $\overline{u'^2}/\Delta U^2$  for a) base line ; b)  $f_e=5\text{Hz}$  ; c)  $f_e=10\text{Hz}$  ; d)  $f_e=60\text{Hz}$  ; e)  $f_e=400\text{Hz}$

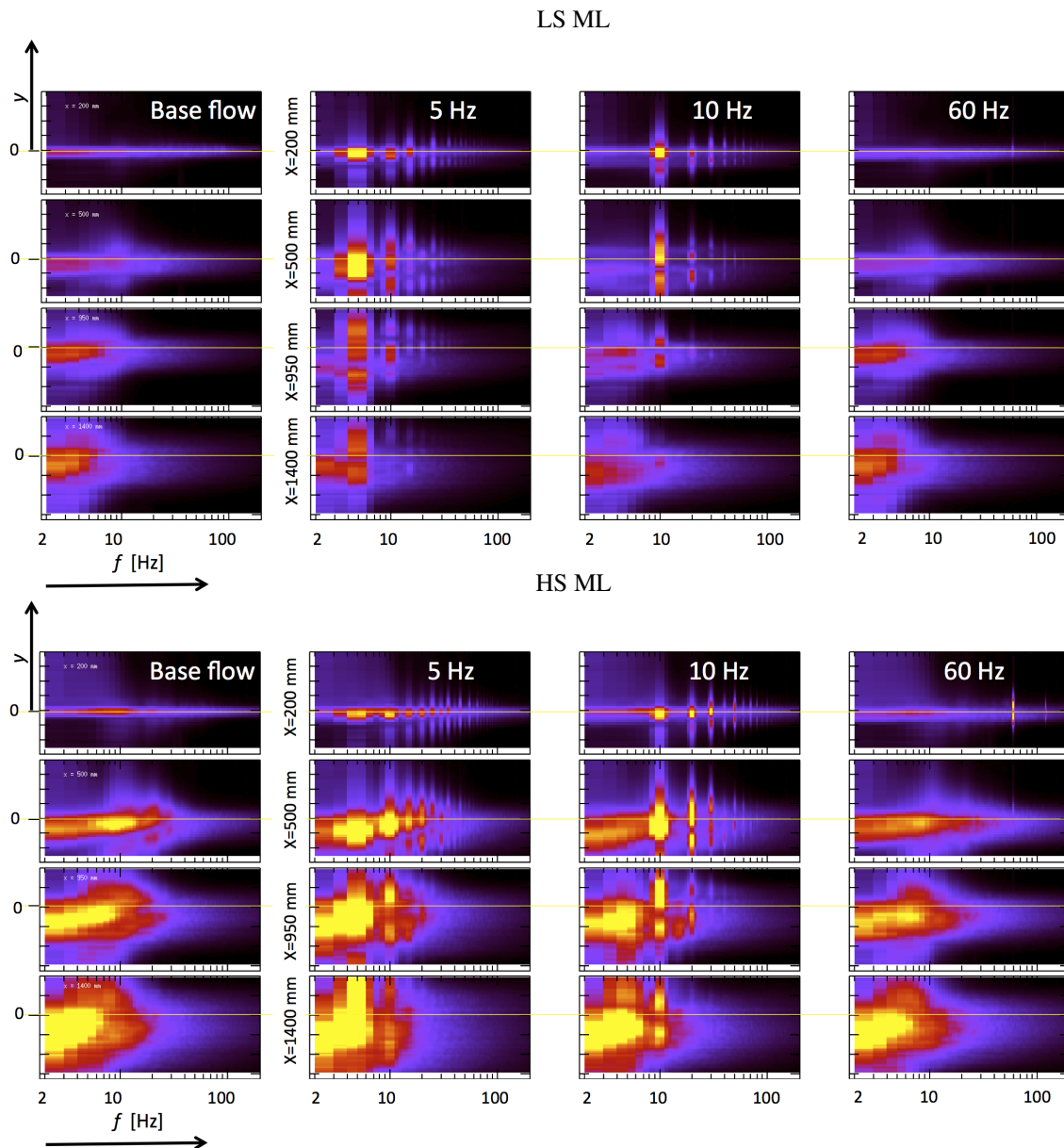


Figure 6. Spectral maps of the energy at actuation frequency  $f_a$  for the low speed (top) and high speed configurations (bottom). The same linear colormap is applied to each plot. Columns correspond the to base line,  $f_a=5$ , 10 and 400 Hz respectively (from left to right).

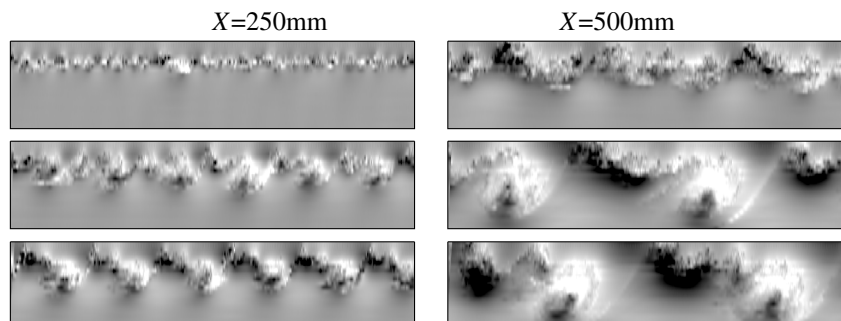


Figure 7. Pseudo Flow Visualisations at  $X = 200$  and  $500$  mm for the low speed LS configuration. Plotted are iso grey levels corresponding to the time history of the fluctuating velocity arising from the hot-wire rake. The vertical direction corresponds to the rake-extent. The horizontal direction corresponds to time ( $0.4$  ms), plotted from right to left, following a Taylor's hypothesis, to match a spatial organisation. Each map is equivalent to a spatial window of size  $\approx 1200 \times 180$  mm<sup>2</sup>. From top to bottom: the base line, the configuration selected by POD feedback, and the harmonic actuation at the dominant frequency arising from the POD feedback.